Engineering 3 (2017) 845–853

Contents lists available at ScienceDirect

Engineering

journal homepage: www.elsevier.com/locate/eng

Research
Bridge Engineering—Article

Investigation of Turbulence Effects on the Aeroelastic Properties of a Truss Bridge Deck Section

Hoang Trong Lam [a], Hiroshi Katsuchi [b,*], Hitoshi Yamada [b]

[a] The University of Danang—University of Science and Technology, Danang, Vietnam
[b] Yokohama National University, Yokohama 240-8501, Japan

ARTICLE INFO

Article history:
Received 10 May 2017
Revised 8 July 2017
Accepted 20 October 2017
Available online 19 December 2017

Keywords:
Flutter derivatives
System identification
Turbulence effect
Buffeting response

ABSTRACT

This paper presents the flutter derivatives (FDs) extracted from a stochastic system identification (SSI) method under different turbulent flows. The objective of the study is to investigate the effects of oncoming turbulence on the flutter of suspended long-span bridges using a section model wind-tunnel test. Several wind-tunnel tests were performed on a truss bridge deck section with different oncoming turbulent properties involving reduced turbulence intensities and turbulent scales. This study includes an investigation of the effect of oncoming flows on modal dynamic responses. The transient and buffeting response data from the wind-tunnel test are analyzed using the system identification technique in extracting FDs, and the difficulties involved in this method are discussed. The time-domain SSI is applied to extract all FDs simultaneously from one and two degree-of-freedom (1DOF and 2DOF) systems. Finally, the results under different conditions are discussed and conclusions are formed.

1. Introduction

Wind flows in the atmospheric boundary layer are always turbulent. Any study of a wind-induced vibration problem must confront this issue, either by matching turbulence characteristics completely or by acknowledging uncertainties in the conclusions as a result of imperfect simulations. Not many studies in this field have focused clearly on the effects of turbulence on aeroelastic forces. Scanlan and Lin [1] are pioneers who used a truss bridge deck section model and concluded that there is an insignificant difference in flutter derivatives (FDs) between smooth and turbulent flows. However, Huston [2] conducted a test on a model of the Golden Gate Bridge deck section and obtained results that were different from those obtained by Scanlan and Lin [1] and Haan and Kareem [3]. In studies on the effect of turbulent flows on FDs, a free-vibration technique using a section model with the application of a system identification technique to extract FDs is widely used. Various system identification techniques have been developed by many authors: These include the extended Kalman filter algorithm [4], the modified Ibrahim time domain (MITD) [5], the unifying least-squares method [6], and the iterative least-squares method [7]. In these systems, buffeting force and its response are considered to be external noise, which causes increased difficulty at high wind velocity. Bartoli and Righi [8] used the combined system identification method (CSIM), which is based on Sarkar's MITD, to simultaneously extract all FDs from a two degrees-of-freedom (2DOF) rectangular section model. Their conclusion was that the identification of FDs in a turbulent flow succeeded in spite of the difficulties caused by locally induced noise due to signature turbulence. The main reason for their success is that the CSIM is a deterministic system identification, and the effects of turbulence are regarded as a noisy-input signal to the system, which results in additional problems in the identification process. Nikitas et al. [9] extracted FDs from ambient vibration data from full-scale monitoring using a more elaborate stochastic identification technique (the covariance block Hankel matrix, CBHM) [10]; that study also illustrated the applicability of system identification techniques to extract valuable results from field measurement data. Kirkegaard and Andersen [11] compared three state-space systems: stochastic subspace system identification (or simply stochastic system identification (SSI)), the matrix block Hankel (MBH) stochastic realization estimator, and the prediction error method (PEM). The SSI was found to give a good result for estimated modal parameters and mode shapes, the MBH was found to give poor estimates of the damping ratios and the mode shapes compared with the other two techniques, and the SSI was found to be approximately ten times faster than the PEM.

* Corresponding author.
E-mail address: katsuchi@ynu.ac.jp (H. Katsuchi).

https://doi.org/10.1016/j.eng.2017.10.001

In addition to the issues described above, there is a shortcoming involved in the free-vibration technique. The extraction of FDs cannot be executed accurately in a high wind speed range because the aerodynamic damping of the vertical mode is too high, and the vertical free-vibration data are rapidly damped out. Based on these considerations, the idea of applying SSI to estimate the FDs from the gust responses of a truss bridge deck section was developed. In this paper, the turbulence effects on the FDs of a truss bridge deck are investigated by employing a section model wind-tunnel test in a turbulent flow. Output-only SSI is applied to extract FDs from gust response. Tests were also carried out using the free-vibration method for comparison with the proposed method.

2. Experimental setup and turbulent flow generation

A wind-tunnel test was conducted in a closed-circuit wind tunnel at Yokohama National University. The working section is 1.8 m wide and 1.8 m high, and the investigated profile is a truss bridge deck section (Fig. 1). It was fabricated from wood with a scale of 1:80 to represent the cross-section of a long-span suspension bridge. The width and depth of the section model are 363 mm and 162.5 mm, respectively. The unit length mass is 8.095 kg·m^{-1} and the unit length moment of inertia is 0.2281 kg·m^2·m^{-1}. The first vertical frequency and damping ratio are 1.869 Hz and 0.00509, respectively, and the first torsional frequency and damping ratio are 3.296 Hz and 0.004186, respectively. The section model was attached to a rigid frame and supported at each corner by a linear spring with stiffness k. The mounting position of the spring was adjusted such that the elastic center and the gravity center of the cross-section coincided. The tests were carried out in both smooth and turbulent flows. The turbulent flows used in this study were generated with a biplane wooden grid, and the turbulent properties were controlled by changing the distance to the model.

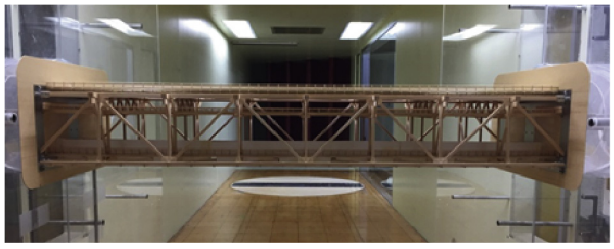

Fig. 1. Truss bridge deck section model.

2.1. Reduced turbulence intensity

For the purpose of matching the power spectrum of the turbulent flow of a model with that of the full-scale version, Katsuchi and Yamada [12] introduced the concept of reduced turbulence intensity (I_r), which can be written as follows:

$$I_r = \frac{I_u}{\left(L_u^x/D\right)^{1/3}} \tag{1}$$

where I_u is the along-wind turbulence intensity, defined by $I_u = \sigma_u/U$, for which σ_u is the standard deviation of the turbulent wind velocity and U is the mean wind velocity; D is the height of the section model; and L_u^x is the integral length scale for the turbulent component in the longitudinal direction. In this study, the integral length scale is defined by

$$L_u^x = \frac{1}{2\pi}\frac{U}{n_{peak}} \tag{2}$$

where n_{peak} is the frequency at which the reduced power spectrum reaches the maximum.

Table 1 depicts the results of three turbulent flow parameters, I_u, L_u^x, and I_r, corresponding to different grid-to-model distances. I_r increases proportionally with I_u, but the inverse is true for L_u^x.

2.2. Power spectral density

The turbulence intensity and the integral length scale do not fully describe the properties of oncoming turbulent flows. Nakamura and Ozono [13] showed that small-scale turbulence affects flow fields and aerodynamic parameters more than large-scale turbulence. Therefore, the power spectral density (PSD) of the turbulence was also quantified for this research. Fig. 2(a) shows the non-dimensional PSD function of the along-wind turbulence, together with the von Karman and Eurocode 1 spectra. Compared with the von Karman spectrum, the measured data coincided well in the high-frequency range and was a little higher in the low-frequency range. Turbulent energy is generated in larger eddies (low frequency). For most structures, these low-frequency

Table 1
Turbulent flow parameters.

Parameter	Case 1	Case 2	Case 3
I_u (%)	6.17	9.11	15.63
L_u^x (cm)	11.26	9.04	6.79
I_r (%)	6.97	11.09	21.02

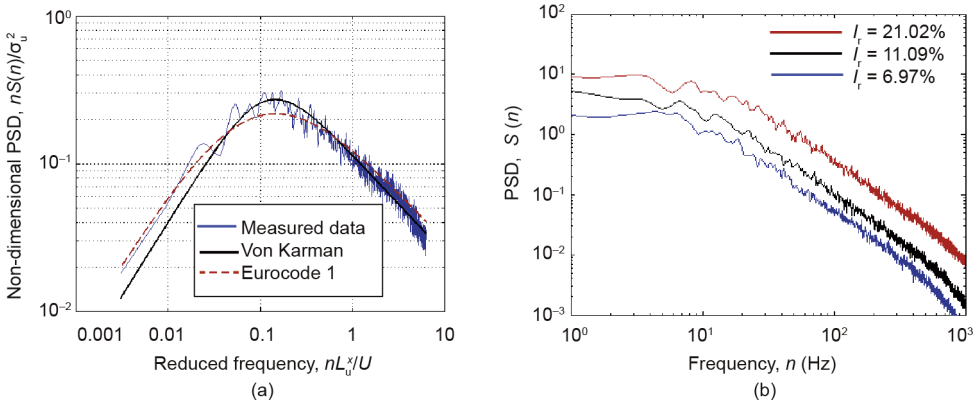

Fig. 2. PSD function for the longitudinal turbulence component. (a) Comparison with proposed formulas; (b) PSD at different I_r.

fluctuations give no significant response contribution. Fig. 2(b) shows three spectra obtained at different I_r. The values of the PSD function increase as I_r increases.

3. Model dynamic responses

Tests were conducted in both smooth and turbulent flows. The objective of this test was to quantify the effect of oncoming turbulent flows on the dynamic responses of the section model.

Fig. 3 illustrates the vibration amplitudes of 2DOF (heaving and torsional modes) versus the reduced wind velocities ($V_r = U/fB$, where f is the frequency and B is the width of the section model) under smooth and various turbulent flows. In smooth flow, vertical vibration is limited when V_r ranges from 0 to 9, and then increases considerably; however, vertical divergent vibration does not occur in this test (Fig. 3(a)). On the other hand, the torsional displacement is very small until a sudden increase and flutter occur at a V_r of about 5.7 (Fig. 3(b)).

When the model is immersed in turbulent flows, vertical and torsional motions appear in spite of small reduced wind velocities. The vertical response increases proportionally with V_r, and when the I_r increases, the amplitude of vibration increases slightly. In the turbulent flows, vertical divergent vibration does not occur. In the cases of $I_r = 6.97\%$ and $I_r = 11.09\%$, the torsional displacement gradually increases with V_r and flutter occurs at $V_r = 7.2$ and $V_r = 7.7$, respectively. The flutter speeds are higher than those in smooth flow ($V_r = 5.7$). Moreover, in the case of $I_r = 21.02\%$, flutter occurs at $V_r = 8.6$. (The critical wind speed is defined at the amplitude of 0.5°.)

In general, turbulent flows on a section model induce larger vibration than smooth flow, and the vibration proportionally increases with the wind velocities; however, the vibration does not suddenly increase in turbulent flows as it does in smooth flow. The motion under turbulent flows is known as buffeting response; it affects the service state of bridges by causing issues such as fatigue problems.

4. Identification of flutter derivatives

In this study, the FDs of a bridge deck in turbulence are identified using an SSI method. The theories applied in this study are mainly based on the work of Peeters and Roeck [14].

4.1. Stochastic state-space models

When considering a 2DOF section model of a bridge deck in turbulent flow, fluctuating wind loads that act on the deck can be expressed by the linear superposition of a self-excited force and a buffeting force as follows:

$$\begin{aligned} m(\ddot{h} + 2\xi_h\omega_h\dot{h} + \omega_h^2 h) &= L_{se} + L_b \\ I(\ddot{\alpha} + 2\xi_\alpha\omega_\alpha\dot{\alpha} + \omega_\alpha^2\alpha) &= M_{se} + M_b \end{aligned} \tag{3}$$

where m and I are the mass and polar moment of the inertial per unit length, respectively; h and α are heaving and torsional displacement, respectively; $(\cdot)$ represents time differentiation; $\omega_h = 2\pi f_h$ and $\omega_\alpha = 2\pi f_\alpha$ are the natural circular frequencies of the heaving and torsional mode, respectively; ξ_h and ξ_α are the damping ratio of heaving and torsion, respectively; L_b and M_b are the buffeting forces in the vertical and torsional directions, respectively; and L_{se} and M_{se} are the self-excited lift and pitching moment, respectively, given by

$$\begin{aligned} L_{se} &= \frac{1}{2}\rho U^2 B\left[K_h H_1^*(K_h)\frac{\dot{h}}{U} + K_\alpha H_2^*(K_\alpha)\frac{B\dot{\alpha}}{U} + K_\alpha^2 H_3^*(K_\alpha)\alpha + K_h^2 H_4^*(K_h)\frac{h}{B}\right] \\ M_{se} &= \frac{1}{2}\rho U^2 B^2\left[K_h A_1^*(K_h)\frac{\dot{h}}{U} + K_\alpha A_2^*(K_\alpha)\frac{B\dot{\alpha}}{U} + K_\alpha^2 A_3^*(K_\alpha)\alpha + K_h^2 A_4^*(K_h)\frac{h}{B}\right] \end{aligned} \tag{4}$$

where ρ is the air density, U is the mean wind velocity, B is the width of the bridge deck, $K_k = \omega_k B/U$ is the reduced frequency (where $k = h, \alpha$), and H_i^* and A_i^* (where $i = 1, 2, 3, 4$) are the FDs.

By substituting Eq. (4) into Eq. (3) and moving the aerodynamic damping and stiffness terms to the left-hand side, Eq. (3) can be rewritten as follows:

$$M\ddot{q}(t) + C^e\dot{q}(t) + K^e q(t) = f(t) = B_2\boldsymbol{u}(t) \tag{5}$$

where $q(t) = [h(t) \quad \alpha(t)]^T$ is the generalized buffeting response, $f(t) = [L_b \quad M_b]^T$ is the buffeting force, $f(t)$ is factorized into matrix B_2 and input vector $\boldsymbol{u}(t)$, M is the mass matrix, C^e is the total damping matrix including the structural and aerodynamic damping, and K^e is the total stiffness matrix including the structural stiffness and aerodynamic stiffness.

The second-order differential equation, Eq. (5), can be transformed into a first-order state equation, Eq. (6):

$$\dot{\boldsymbol{x}}(t) = A_c\boldsymbol{x}(t) + B_c\boldsymbol{u}(t) \tag{6}$$

where

$$\boldsymbol{x}(t) = \begin{bmatrix} q(t) \\ \dot{q}(t) \end{bmatrix}, \quad A_c = \begin{bmatrix} 0 & I_u \\ -M^{-1}K^e & -M^{-1}C^e \end{bmatrix}, \quad B_c = \begin{bmatrix} 0 \\ M^{-1}B_2 \end{bmatrix}$$

and where A_c is the designated state matrix with a size of 4×4, $\boldsymbol{x}(t)$ is the state vector, B_c is the input matrix, and I_u is a unit matrix.

The combination of the state equation and the observation equation fully describe the input and output behaviors of the structural system; as such, it is named the *state-space system*.

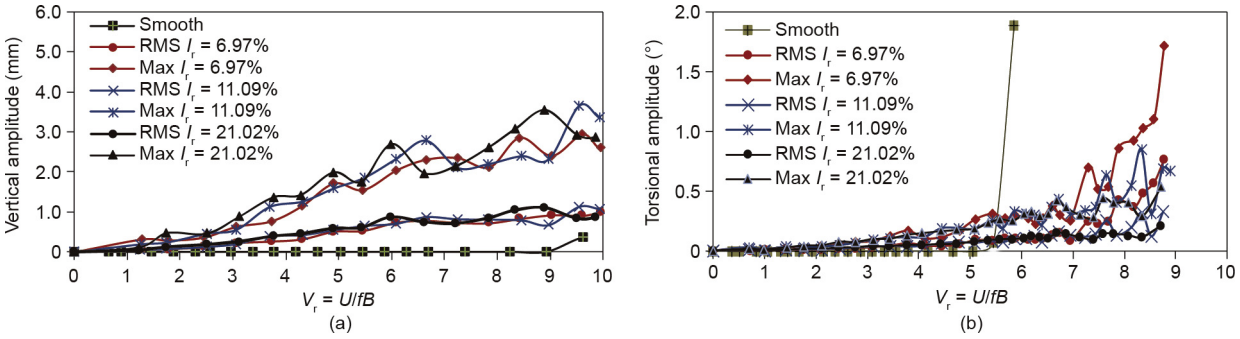

Fig. 3. Model response with different I_r. (a) Vertical amplitude; (b) torsional amplitude. Note that RMS refers to the root-mean-square, "Max" is the maximum amplitude of vibration, and "Smooth" is the smooth flow condition.

$$\begin{aligned}\dot{\boldsymbol{x}}(t) &= A_c\boldsymbol{x}(t) + B_c\boldsymbol{u}(t)\\ \boldsymbol{y}(t) &= C_c\boldsymbol{x}(t) + D_c\boldsymbol{u}(t)\end{aligned} \tag{7}$$

where $\boldsymbol{y}(t)$ is the output vector, C_c is the output matrix, and D_c is the direct transmission matrix in continuous time.

Eq. (7) is a deterministic state-space model in continuous time. *Continuous time* implies that the expression can be evaluated at each time instant. *Deterministic* implies that the input and output quantities can be measured exactly. This is not practical, because the measurements are mostly sampled at a discrete time. In addition, it is impossible to measure all DOFs, and measurements always cause disturbance effects. For all these reasons, the continuous deterministic system is converted into a suitable form—that of a discrete-time stochastic state-space model—as follows:

$$\begin{aligned}x_{k+1} &= Ax_k + w_k\\ y_k &= Cx_k + v_k\end{aligned} \tag{8}$$

where $x_k = x(k\Delta t) = (\,q_k \quad \dot{q}_k\,)^{\mathrm{T}}$ is the discrete-time state vector containing the discrete sampled displacement q_k and velocity $\dot{q}_k$; w_k is the process noise due to disturbances and modeling error; v_k is the measurement noise due to sensor inaccuracy; and A and C are discrete state and output matrices, respectively. It is assumed that w_k and v_k are zero mean and that their covariance matrix is as follows:

$$E\left[\begin{pmatrix} w_p \\ v_p \end{pmatrix}\begin{pmatrix} w_q^{\mathrm{T}} & v_q^{\mathrm{T}} \end{pmatrix}\right] = \begin{bmatrix} Q & S \\ S^{\mathrm{T}} & R \end{bmatrix}\delta_{pq} \tag{9}$$

where the indices p and q are time instants, E is the expectation operator, and δ_{pq} is the Kronecker delta. The correlations $E[\,w_p \quad w_q^{\mathrm{T}}\,]$ and $E[\,v_p \quad v_q^{\mathrm{T}}\,]$ are equal to zero in the case of different time instants. $Q = E[\,w_k \quad w_k^{\mathrm{T}}\,]$, $R = E[\,v_k \quad v_k^{\mathrm{T}}\,]$, and $S = E[\,w_k \quad v_k^{\mathrm{T}}\,]$. It is further assumed that the stochastic model x_k, w_k, and v_k are mutually independent and zero mean. It can be proven that the output covariance $R = E[\,y_{k+1} \quad y_k^{\mathrm{T}}\,]$ for any arbitrary time-lags $i\Delta t$ can be regarded as the impulse response of the deterministic linear time-invariant system A, C, G, where $G = E[\,x_{k+1} \quad y_k^{\mathrm{T}}\,]$ is the next state-output covariance matrix, as shown in Eq. (10).

$$R_i = CA^{i-1}G \tag{10}$$

Eq. (10) is called the Lyapunov equation, and indicates that the output covariance can be regarded as impulse responses. Therefore, the theoretical application of the stochastic system can go back to an eigensystem realization algorithm (ERA) method [15].

4.2. Data-driven stochastic system identification

The output measurement data obtained from l sensors (in this study, $l = 2$ for heaving and torsion) are as follows:

$$y = (y_0, y_1, y_2, \ldots, y_n) \in \mathbb{R}^{l\times n} \tag{11}$$

The output data are assembled in a block Hankel matrix (H) with $2i$ block rows and j columns. The Hankel matrix can be divided into two parts: The upper part is the past output and the lower is the future output, as follows:

$$H = \left[\begin{array}{cccc} y_0 & y_1 & \cdots & y_{j-1} \\ y_1 & y_2 & \cdots & y_j \\ \vdots & \vdots & \ddots & \vdots \\ \hline y_{i-1} & y_i & \cdots & y_{i+j-2} \\ y_i & y_{i+1} & \cdots & y_{i+j-1} \\ y_{i+1} & y_{i+2} & \cdots & y_{i+j} \\ \vdots & \vdots & \ddots & \vdots \\ y_{2i-1} & y_{2i} & \cdots & y_{2i+j-2} \end{array}\right]_{2i\times j} = \begin{bmatrix} Y_{0|i-1} \\ \hline Y_{i|2i-1} \end{bmatrix} = \begin{bmatrix} Y_p \\ \hline Y_f \end{bmatrix} \begin{matrix} \updownarrow li \\ \hline \updownarrow li \end{matrix} \tag{12}$$

Like the CBHM or ERA method, data-driven stochastic system identification (SSI_data) implements directly with the output of experimental data, without converting output data to correlation, covariance, or spectra [16]. The main step of SSI_data is a projection of the row space of the future outputs (Y_f) into the row of past outputs ($\boldsymbol{Y}_p$). The orthogonal projection P_i is defined as follows:

$$P_i = Y_f/\boldsymbol{Y}_p = Y_f Y_p (Y_p Y_p^{\mathrm{T}})^{-1} Y_p \tag{13}$$

The orthogonal projection is implemented by the QR factorization of the block Hankel matrix shown in Eq. (12). This is defined as follows:

$$H = \begin{bmatrix} Y_p \\ \hline Y_f \end{bmatrix} = RQ^{\mathrm{T}} \tag{14}$$

where $Q \in \mathbb{R}^{j\times j}$ is an orthogonal matrix $Q^{\mathrm{T}}Q = QQ^{\mathrm{T}} = I_j$ and $R \in \mathbb{R}^{2li\times j}$ is a lower triangular matrix. Because $2li < j$, it is possible to reject the zeros in R and the corresponding zeros in Q.

$$H = \begin{array}{c} \\ li \\ l \\ l(i-1) \end{array} \begin{array}{c} \begin{matrix} li & l & l(\mathrm{i}-1) & j\to\infty \\ \leftrightarrow & \leftrightarrow & \leftrightarrow & \leftrightarrow \end{matrix} \\ \begin{bmatrix} R_{11} & 0 & 0 \\ R_{21} & R_{22} & 0 \\ R_{31} & R_{32} & R_{33} \end{bmatrix} \end{array} \begin{array}{c} \begin{bmatrix} Q_1^{\mathrm{T}} \\ Q_2^{\mathrm{T}} \\ Q_3^{\mathrm{T}} \end{bmatrix} \\ \begin{matrix} \updownarrow li \\ \updownarrow l \\ \updownarrow l(i-1) \end{matrix} \end{array} \tag{15}$$

Substituting the QR factorization of the output Hankel matrix, Eq. (15), into Eq. (13) yields the simple expression of the projection:

$$P_i = \begin{bmatrix} R_{21} \\ R_{31} \end{bmatrix} Q_1^{\mathrm{T}} \tag{16}$$

The key of SSI is that the orthogonal projection P_i is factorized into the product of the observability matrix O_i and the Kalman filter state sequence $\hat{X}_i$.

$$P_i = \begin{bmatrix} C \\ CA \\ \vdots \\ CA^{i-1} \end{bmatrix} \begin{bmatrix} \hat{x} & \hat{x}_{i+1} & \cdots & \hat{x}_{i+j-1} \end{bmatrix} = O_i\hat{X}_i \tag{17}$$

The observability matrix O_i and the Kalman filter sequence $\hat{X}_i$ are obtained by applying single-value decomposition to the projection matrix:

$$P_i = U_1 S_1 V_1^{\mathrm{T}} \tag{18}$$

Comparing Eq. (17) and Eq. (18) gives

$$O_i = U_1 S_1^{1/2}, \quad \hat{X}_i = O_i^{\dagger} P_i \tag{19}$$

where $(\cdot)^{\dagger}$ represents the pseudo-inverse of a matrix.

If the past and future outputs of the Hankel matrix are shifted, a time-shift projection is achieved:

$$P_{i-1} = Y_f^{-}/\boldsymbol{Y}_p^{+} = O_{i-1}\hat{X}_{i+1} \tag{20}$$

where

$$P_{i-1} = \begin{bmatrix} R_{31} & R_{32} \end{bmatrix} \begin{bmatrix} Q_1^{\mathrm{T}} \\ Q_2^{\mathrm{T}} \end{bmatrix} \tag{21}$$

O_{i-1} is obtained from O_i after deleting the last l rows. The shifted state sequence can be computed in Eq. (20) as follows:

$$\hat{X}_{i+1} = O_{i-1}^{\dagger} P_{i-1} \tag{22}$$

From Eq. (19) and Eq. (22), the Kalman state sequences $\hat{X}_i$ and $\hat{X}_{i+1}$ are obtained using only output data. The state and controllability matrices can be recovered from the over-determined set of linear equations, obtained by extending Eq. (8):

$$\begin{bmatrix}\hat{X}_{i+1}\\ Y_{i|i}\end{bmatrix}=\begin{bmatrix}A\\ C\end{bmatrix}\hat{X}_i+\begin{bmatrix}\rho_w\\ \rho_v\end{bmatrix}$$
$$Y_{i|i}=\begin{bmatrix}R_{21} & R_{22}\end{bmatrix}\begin{bmatrix}Q_1^{\mathrm{T}}\\ Q_2^{\mathrm{T}}\end{bmatrix} \quad (23)$$

where $Y_{i|i}$ is a Hankel matrix with only one block row. Since the Kalman state sequence and the outputs are known, and the residual $[\rho_w^{\mathrm{T}} \quad \rho_v^{\mathrm{T}}]^{\mathrm{T}}$ are uncorrelated with $\hat{X}_i$, the set of equations can be solved for A and C using the least-squares method:

$$\begin{bmatrix}A\\ C\end{bmatrix}=\begin{bmatrix}\hat{X}_{i+1}\\ Y_{i|i}\end{bmatrix}\left[\hat{X}_i\right]^{\dagger} \quad (24)$$

4.3. Identification of flutter derivatives

The modal parameters of the system can be obtained by solving the eigenvalue problem for the state matrix:

$$A=\boldsymbol{\Psi}\Lambda\boldsymbol{\Psi}^{-1},\quad \Phi=C\boldsymbol{\Psi} \quad (25)$$

where $\boldsymbol{\Psi}$ is the complex eigenvector, Λ is the complex eigenvalue and the diagonal matrix, and Φ is the mode shape matrix. When the complex modal parameters are known, the total damping matrix C^{e} and total stiffness matrix K^{e} in Eq. (5) are determined by

$$\begin{bmatrix}\mathrm{K}^{\mathrm{e}} & C^{\mathrm{e}}\end{bmatrix}=-M\begin{bmatrix}\Phi\Lambda^2 & \Phi^*(\Lambda^*)^2\end{bmatrix}\begin{bmatrix}\Phi & \Phi^*\\ \Phi\Lambda & \Phi^*\Lambda^*\end{bmatrix}^{-1} \quad (26)$$

Let $\bar{C}^{\mathrm{e}}=M^{-1}C^{\mathrm{e}},\bar{K}^{\mathrm{e}}=M^{-1}K^{\mathrm{e}},\bar{C}=M^{-1}C^0,\bar{K}=M^{-1}K^0$, where C^0 and K^0 are the structural damping and stiffness matrix of the system, respectively, under still air conditions.

Thus, the FDs of a 2DOF system can be defined as follows:

$$\begin{aligned}
H_1^*(K_h)&=-\frac{2m}{\rho B^2\omega_h}(\bar{C}_{11}^{\mathrm{e}}-\bar{C}_{11}),\quad A_1^*(K_h)=-\frac{2I}{\rho B^3\omega_h}(\bar{C}_{21}^{\mathrm{e}}-\bar{C}_{21})\\
H_2^*(K_\alpha)&=-\frac{2m}{\rho B^3\omega_\alpha}(\bar{C}_{12}^{\mathrm{e}}-\bar{C}_{12}),\quad A_2^*(K_\alpha)=-\frac{2I}{\rho B^4\omega_\alpha}(\bar{C}_{22}^{\mathrm{e}}-\bar{C}_{22})\\
H_3^*(K_\alpha)&=-\frac{2m}{\rho B^3\omega_\alpha^2}(\bar{K}_{12}^{\mathrm{e}}-\bar{K}_{12}),\quad A_3^*(K_\alpha)=-\frac{2I}{\rho B^4\omega_\alpha^2}(\bar{K}_{22}^{\mathrm{e}}-\bar{K}_{22})\\
H_4^*(K_h)&=-\frac{2m}{\rho B^3\omega_h^2}(\bar{K}_{11}^{\mathrm{e}}-\bar{K}_{11}),\quad A_4^*(K_h)=-\frac{2I}{\rho B^4\omega_h^2}(\bar{K}_{21}^{\mathrm{e}}-\bar{K}_{21})
\end{aligned} \quad (27)$$

5. Flutter derivatives and comparison

The buffeting and decay responses were acquired at a sampling frequency of 100 Hz. Fig. 4 shows the time-history responses of the model at the mean wind speed of 6.7 m·s^{-1}.

5.1. Extraction of flutter derivatives from buffeting response

In a high wind speed range, the aerodynamic damping of the heaving mode is too high and the vertical free response is too short, so the extraction of FDs cannot be accomplished with high accuracy. In addition, it is not practical to use a free-decay mechanism to describe real bridge behavior under field wind excitation. On the other hand, the extraction of FDs from the buffeting response more closely reflects full-scale bridge behavior in a turbulent wind field. The bridge deck section model will vibrate under the excitation of turbulent flow even at a low wind velocity.

This method is simpler than the free-vibration technique because no operator corrupts by exciting the section model. Fig. 5 and Fig. 6 show the FDs of the bridge deck extracted by the SSI_data method from both the free-decay and buffeting responses of 1DOF and 2DOF systems under turbulence flows (I_{r} = 11.09%). In general, most FDs are in good agreement with both the free-decay response and the buffeting response of 1DOF and 2DOF systems. The heaving-related damping FD (H_1^*) extracted from the buffeting response is slightly higher than that obtained from the free-decay response. The coupled terms (H_2^* and H_3^*) extracted from buffeting responses are more scattered than those from free-decay responses, particularly at a highly reduced wind velocity. The trends for A_3^* of the FDs are similar in both cases. In this study, the sectional profile was a truss bridge deck section where only torsional flutter occurred; therefore, A_2^* is the most important derivative. The A_2^* extracted from the buffeting response is scattered at low reduced wind velocities, but the scatter decreases more at a high reduced wind velocity for the buffeting response than for the free-decay response. The trends of the results from the buffeting response and free-decay response are closely coincident.

5.2. The effects of turbulence on flutter derivatives

Fig. 7 and Fig. 8 illustrate the FDs of the heaving and torsional modes under smooth and turbulent flows with different I_{r}. It was

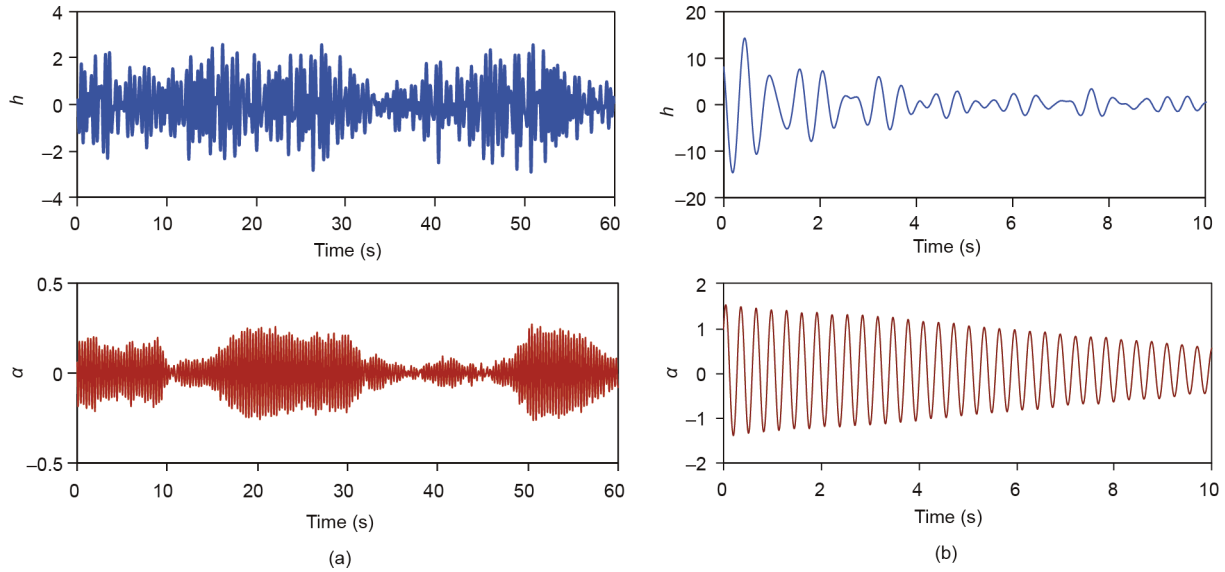

Fig. 4. Responses of the bridge deck section model (h is vertical and α is torsional). (a) Buffeting response (U = 6.7 m·s^{-1}); (b) free-decay response (U = 6.7 m·s^{-1}).

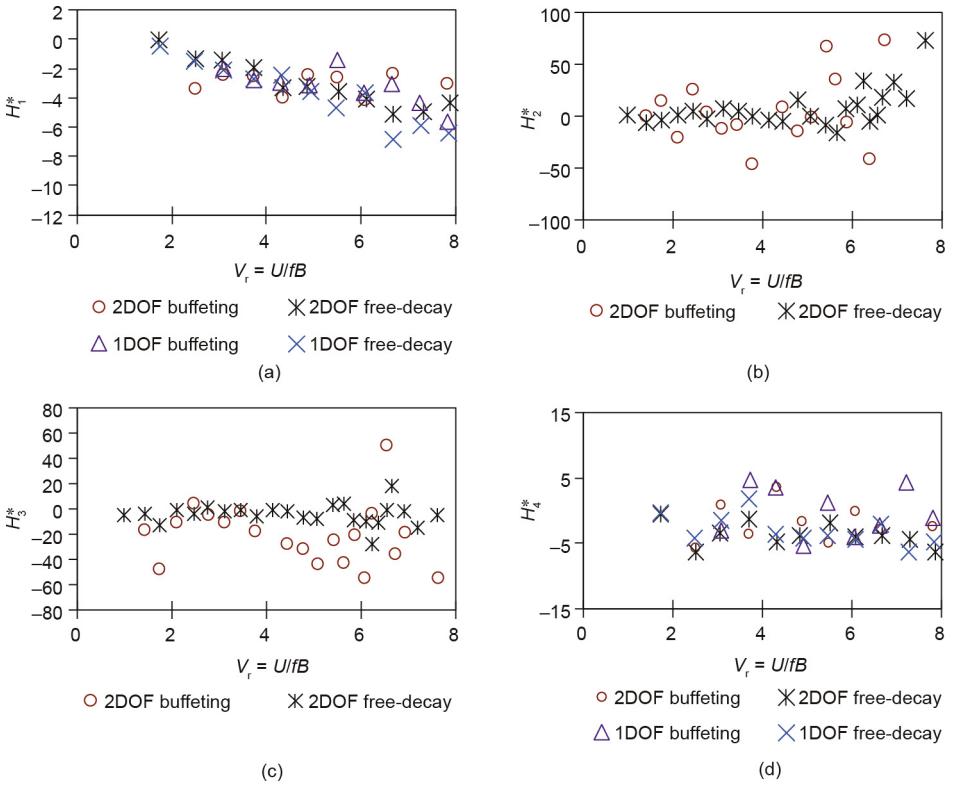

Fig. 5. Heaving mode FDs (H_i^*) of the bridge deck section model from 1DOF and 2DOF tests by free-decay and buffeting responses (I_r = 11.09%). (a) H_1^*; (b) H_2^*; (c) H_3^*; (d) H_4^*.

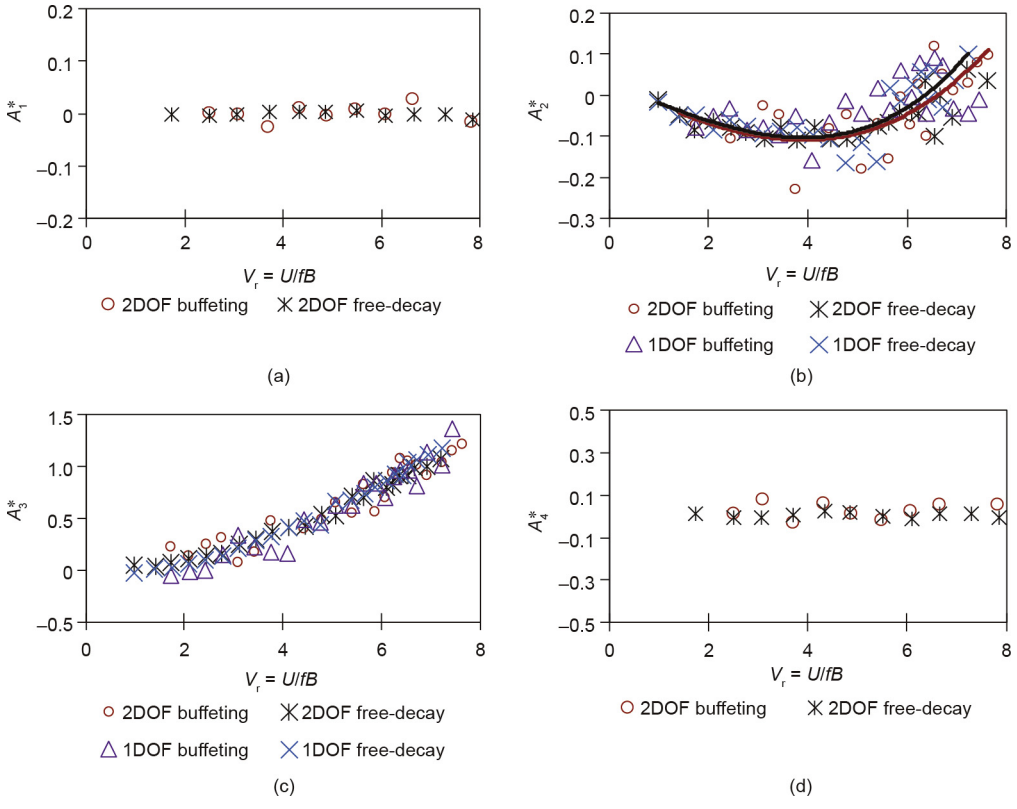

Fig. 6. Torsional mode FDs (A_i^*) of the bridge deck section model from 1DOF and 2DOF tests by free-decay and buffeting responses (I_r = 11.09%). (a) A_1^*; (b) A_2^*; (c) A_3^*; (d) A_4^*. Black and red lines are the curve fitting of the 2DOF free-decay and 2DOF buffeting responses, respectively.

found that under smooth flow, the FD H_1^* decreases faster than that under turbulent flows. This is because the damping ratio of the heaving mode under smooth flow is higher than under turbulent flow. Turbulence has a very small effect on the vertical and torsional frequency terms H_4^* and A_3^*, and these values extracted from the buffeting response are somewhat lower in turbulence than in smooth flow. The off-diagonal terms H_2^*, H_3^*, A_1^*, and A_4^* fluctuate around zero, which means that in this experiment, coupled vibra-

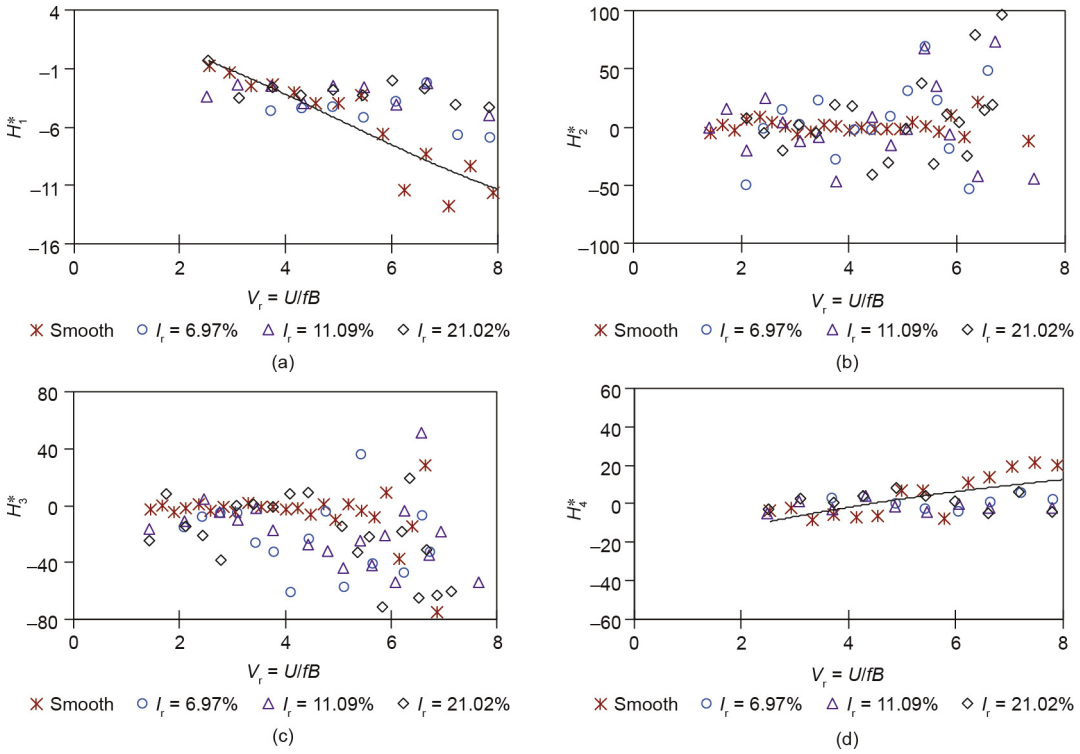

Fig. 7. Heaving mode FDs (H_i^*) of the bridge deck section model under smooth and turbulent flows by buffeting response. (a) H_1^*; (b) H_2^*; (c) H_3^*; (d) H_4^*. The solid curve is the fitted polynomial of the smooth case.

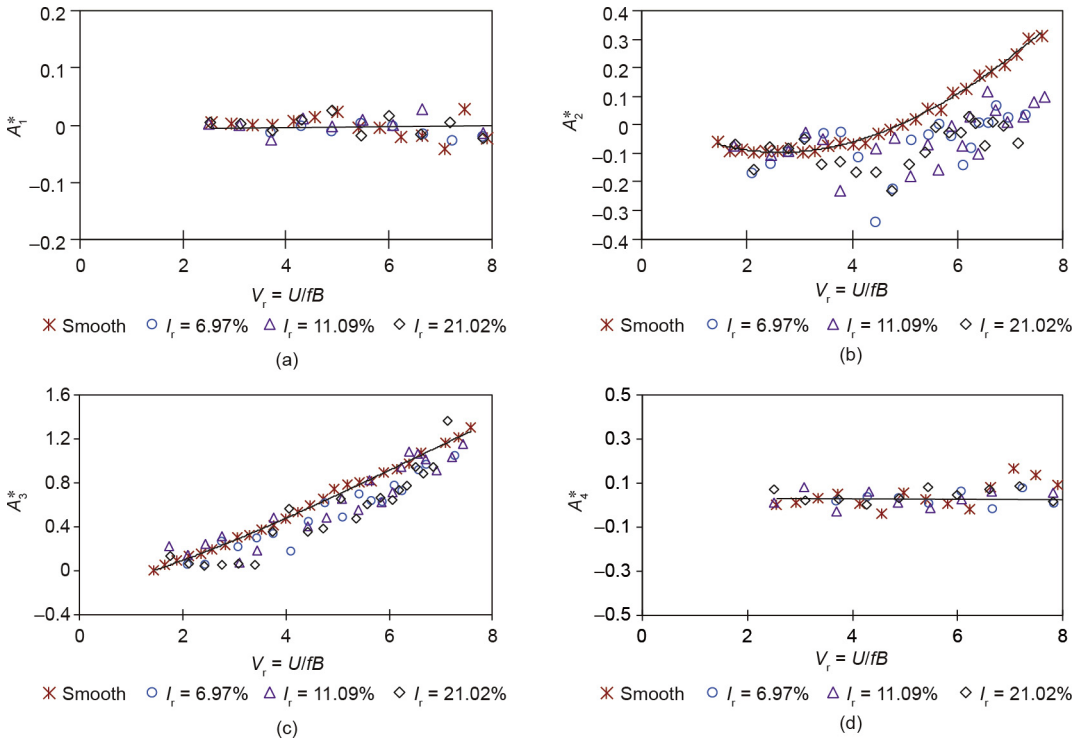

Fig. 8. Torsional mode FDs (A_i^*) of the bridge deck section model under smooth and turbulent flows by buffeting response. (a) A_1^*; (b) A_2^*; (c) A_3^*; (d) A_4^*. The solid curves are the fitted polynomials of the smooth case.

tion did not appear. Of these derivatives, the torsional damping term A_2^* plays an important role in torsional flutter stability, since its positive/negative value corresponds to the aerodynamic instability/stability of the torsional flutter. As shown in Fig. 8, under smooth flow, A_2^* is positive at high reduced wind velocity $V_r = 5.2$ and coincides with the negative total torsional damping. The significant effects of turbulent flows on FDs are particularly illustrated for the aerodynamic torsional damping term A_2^*: The positive value corresponds to a V_r of around 6.5–7.8 under $I_r = 6.97\%$ and $I_r = 11.09\%$, respectively, whereas in the case of $I_r = 21.02\%$, flutter does not occur up to $V_r = 8$. On the other hand, the effects of different turbulent intensities on FDs are fairly modest. The influence of turbulence on FDs will depend on the section. Sarkar et al. [5] found a small effect for a streamlined section, whereas the test on a truss bridge deck showed an appreciable effect, which is clearly shown by the torsional damping term A_2^* .

There are two factors that may affect FDs in a turbulent flow: the spanwise turbulence coherence and the aerodynamic admittance. In Fig. 7 and Fig. 8, turbulence effects can be seen in some FD terms. Significantly different trends can be seen in the diagonal terms (H_1^*, H_4^*, A_2^*, and A_3^*) of the smooth and turbulent flows. On the other hand, this difference is not significant in Fig. 5 and Fig. 6, where different identification procedures (buffeting/free decay) were applied for the same turbulence. It may be concluded from these observations that aerodynamic admittance causing a buffeting response does not significantly affect FD identification, although the difference in spanwise turbulence coherence between smooth and turbulent flows does have a significant effect on FD identification.

5.3. Flutter critical wind velocity

In order to confirm the results of identified FDs under buffeting responses, the flutter critical wind velocity (V_{cr}) was obtained from an equation of motion of a 2DOF system:

$$M\ddot{q} + C\dot{q} + Kq = F\ddot{q} \tag{28}$$

where $M = \begin{bmatrix} m & 0 \\ 0 & I \end{bmatrix}$, $C = \begin{bmatrix} 2m\xi_h\omega_h & 0 \\ 0 & 2I\xi_\alpha\omega_\alpha \end{bmatrix}$, $K = \begin{bmatrix} m\omega_h^2 & 0 \\ 0 & I\omega_\alpha^2 \end{bmatrix}$, $F = \begin{bmatrix} L_h & L_\alpha \\ M_h & M_\alpha \end{bmatrix}$, and $q = \begin{bmatrix} h \\ \alpha \end{bmatrix}$.

For a stability check, only the self-excited force is considered, and L_h, L_α, M_h, and M_α are self-excited force components defined by

$$\begin{aligned} L_h &= -\pi\rho B^2(L_{h\mathrm{R}} + iL_{h\mathrm{I}}), \quad L_\alpha = -\pi\rho B^2(L_{\alpha\mathrm{R}} + iL_{\alpha\mathrm{I}}) \\ M_h &= -\pi\rho B^4(M_{h\mathrm{R}} + iM_{h\mathrm{I}}), \quad M_\alpha = -\pi\rho B^4(M_{\alpha\mathrm{R}} + iM_{\alpha\mathrm{I}}) \end{aligned} \tag{29}$$

where $L_{h\mathrm{R}}$, $L_{h\mathrm{I}}$, $L_{\alpha\mathrm{R}}$, $L_{\alpha\mathrm{I}}$, $M_{h\mathrm{R}}$, $M_{h\mathrm{I}}$, $M_{\alpha\mathrm{R}}$, and $M_{\alpha\mathrm{I}}$ are self-excited force coefficients (FDs) that can be compared with those using Scanlan's format, as follows:

$$\begin{aligned} L_{h\mathrm{R}} &= H_4^*/2\pi, \quad L_{h\mathrm{I}} = H_1^*/2\pi, \quad L_{\alpha\mathrm{R}} = H_3^*/2\pi, \quad L_{\alpha\mathrm{I}} = H_2^*/2\pi \\ M_{h\mathrm{R}} &= A_4^*/2\pi, \quad M_{h\mathrm{I}} = A_1^*/2\pi, \quad M_{\alpha\mathrm{R}} = A_3^*/2\pi, \quad M_{\alpha\mathrm{I}} = A_2^*/2\pi \end{aligned} \tag{30}$$

The FDs of the truss bridge deck section that are provided in this study were approximated polynomials of the results from Fig. 7 and Fig. 8.

Assuming sinusoidal motion $q = q_0\exp(i\omega t)$, and since structural damping of a long-span bridge can be negligibly small, the damping matrix in Eq. (28) can be dropped. The aerodynamically influenced equation of motion can then be written as follows:

$$K^{-1}(M - F)\ddot{q} = \frac{1}{\omega^2}\ddot{q} \tag{31}$$

Solving Eq. (31) as an eigenvalue problem gives the stability condition of the system. Fig. 9 shows the change in the aerodynamic damping of the torsional mode. The flutter critical wind velocity is defined as the cross point of the torsional aerodynamic logarithmic decrement and the equivalent torsional structural logarithmic decrement ($\delta = -0.0263$). The flutter critical wind velocity found from the FDs coincided with that found using a wind-tunnel

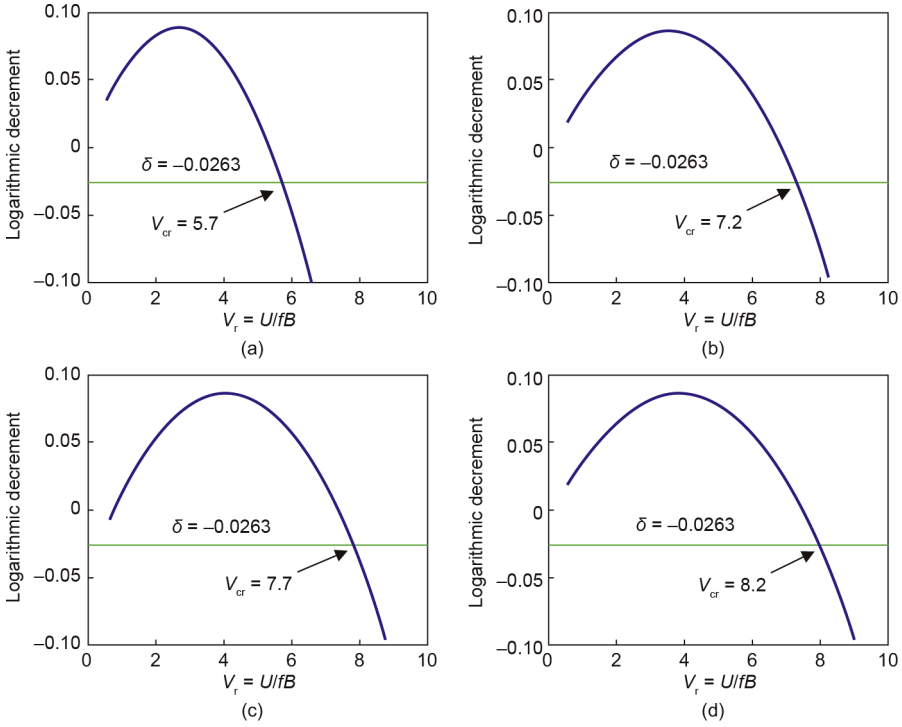

Fig. 9. Change of total logarithmic decrement and flutter critical wind velocity. (a) Smooth flow; (b) $I_r = 6.97\%$; (c) $I_r = 11.09\%$; (d) $I_r = 21.02\%$.

dynamic test (Fig. 3). In the case of I_r = 21.02%, the flutter critical wind velocity identified from the FDs (V_{cr} = 8.2) was slightly smaller than that obtained from the dynamic test (V_{cr} = 8.6).

6. Conclusions

This study investigated the effects of turbulence on the FDs of a truss bridge deck section using a wind-tunnel test and the SSI method. The following conclusions were obtained from this study:

- FDs can be successfully obtained from gust responses. The advantages of this method include the gust response being easy to obtain and this method being less time-consuming than the traditional method; in particular, the length of the time history makes it easy to meet the requirements for extracting FDs, even at a high wind speed—a situation that reflects full-scale bridge behaviors more closely than the traditional method.
- SSI_data shows good results even from gust response because this method holds the advantage of considering buffeting force and response as inputs instead of as noise.
- Turbulent flow significantly affects the dynamic response and FDs of the truss bridge deck section. A_2^* became positive at V_r = 5.2 in the smooth flow and was delayed until V_r = 6.5–7.8 in the turbulent flows of I_r = 6.97% and I_r = 11.09%, respectively; in the case of I_r = 21.02%, a positive value for A_2^* did not appear.

Compliance with ethics guidelines

Hoang Trong Lam, Hiroshi Katsuchi, and Hitoshi Yamada declare that they have no conflict of interest or financial conflicts to disclose.

References

[1] Scanlan RH, Lin WH. Effects of turbulence on bridge flutter derivatives. J Eng Mech Div 1978;104(4):719–33.
[2] Huston DR. The effects of upstream gusting on the aeroelastic behavior of long suspended-span bridges [dissertation]. Princeton: Princeton University; 1986.
[3] Haan FL, Kareem A. The effects of turbulence on the aerodynamics of oscillating prisms. In: Proceedings of the 12th international conference on wind engineering; 2007 Jul 1–6. Cairns, Australia. p. 1815–22.
[4] Yamada H, Miyata T, Ichikawa H. Measurement of aerodynamic coefficients by system identification methods. J Wind Eng Ind Aerod 1992;42(1–3):1255–63.
[5] Sarkar PP, Jones NP, Scanlan RH. Identification of aeroelastic parameters of flexible bridges. J Eng Mech 1994;120(8):1718–42.
[6] Gu M, Zhang RX, Xiang HF. Identification of flutter derivatives of bridge decks. J Wind Eng Ind Aerod 2000;84(2):151–62.
[7] Chowdhury AG, Sarkar PP. A new technique for identification of eighteen flutter derivatives using a three-degree-of-freedom section model. Eng Struct 2003;25(14):1763–72.
[8] Bartoli G, Righi M. Flutter mechanism for rectangular prisms in smooth and turbulent flow. J Wind Eng Ind Aerod 2006;94(5):275–91.
[9] Nikitas N, Macdonal JHG, Jakobsen JB. Identification of flutter derivatives from full-scale ambient vibration measurements of the Clifton Suspension Bridge. Wind Struct An Int J 2011;14(3):221–38.
[10] Bogunović Jakobsen J, Hjorth-Hansen E. Determination of the aerodynamic derivatives by a system identification method. J Wind Eng Ind Aerod 1995;57(2–3):295–305.
[11] Kirkegaard PH, Andersen P. State space identification of civil engineering structures from output measurements. In: Proceedings of the 15th international modal analysis conference; 1997 Feb 3–6; Orlando, FL, USA. Aalborg: Department of Building Technology and Structural Engineering, Aalborg University; 1997. p. 889–95.
[12] Katsuchi H, Yamada H. Study on turbulence partial simulation for wind-tunnel testing of bridge deck. In: Proceedings of the 13th international conference on wind engineering, 2011 Jul 10–15. Amsterdam, the Netherlands.
[13] Nakamura Y, Ozono S. The effects of turbulence on a separated and reattaching flow. J Fluid Mech 1987;178:477–90.
[14] Peeters B, Roeck GD. Reference-based stochastic subspace identification for output-only modal analysis. Mech Syst Signal Pr 1999;13(6):855–78.
[15] Juang JN, Pappa RS. An eigensystem realization algorithm (ERA) for modal parameter identification and model reduction. J Guid Control Dynam 1985;8(5):620–7.
[16] Siringoringo DM, Fujino Y. System identification of suspension bridge from ambient vibration response. Eng Struct 2008;30(2):462–77.